Stability of an impulsive control scheme for spacecraft formations in eccentric orbits

Ludwik A Sobiesiak and Christopher Damaren

Proceedings of the Institution of Mechanical Engineers, Part G: Journal of Aerospace Engineering 2013 227: 1646
originally published online 10 October 2012
DOI: 10.1177/0954410012462784

Original Article

Institution of MECHANICAL ENGINEERS
Journal of AEROSPACE ENGINEERING

Proc IMechE Part G:
J Aerospace Engineering
227(10) 1646–1659

DOI: 10.1177/0954410012462784
uk.sagepub.com/jaero
SAGE

Stability of an impulsive control scheme for spacecraft formations in eccentric orbits

Ludwik A Sobiesiak and Christopher Damaren

Abstract

An *N*-impulse control scheme for spacecraft formations in elliptical orbits is developed to regulate the differential elements of the deputy spacecraft in the presence of the J_2 perturbation. The presented control scheme is an extension of an existing circular-orbit formation control scheme and is shown to perform well at large eccentricities where the circular control scheme fails. For the case of two impulses being applied at arbitrary firing times, a discrete-time approach for ascertaining the stability of the controlled spacecraft formation, under the assumption of small impulsive thrusts, is presented. It is found that stability is guaranteed for the majority of firing time pairs; however, the requisite ΔV can be prohibitive for some firing time pairs. The control scheme and stability predictions for formations in high eccentricity orbits are validated in numerical simulation.

Keywords

Spacecraft formation flying, eccentric orbits, impulsive control

Date received: 27 March 2012; accepted: 7 September 2012

Introduction

Spacecraft formation flying is a maturing technology suitable for Earth observation, Earth science, and astronomical science missions. Spacecraft formations in eccentric orbits specifically have been identified as particularly useful for such missions. Both NASA's magnetospheric multiscale (MMS) mission[1] and ESA's PROBA-3 solar coronagraphy mission[2] are planned formation flying missions that will employ highly elliptical orbits to achieve their scientific objectives. When considering spacecraft formations, the motion of one spacecraft (the deputy) is typically considered relative to a reference spacecraft (the chief). Geometries can range from a simple leader-follower formation to a complex multi-spacecraft tetrahedral formation, such as the one being considered for the MMS mission. Periodic formations, such as the projected circular orbit, where the deputy spacecraft appears to circle the chief, are formation geometries currently being considered for distributed synthetic aperture radar applications (SAR). If left uncontrolled, spacecraft formation geometry will degrade due to disturbances that spacecraft are subjected to, such as the J_2 zonal harmonic caused by the Earth's oblateness, solar radiative pressure, atmospheric drag, and third-body gravitational effects. Whatever the geometry of a particular mission, the maintenance of a specific formation geometry is key to a formation flying mission.

This article presents an impulsive formation maintenance strategy based on the control of mean differential orbital elements for spacecraft formations flying in eccentric orbits. The strategy is suitable for an arbitrary number of corrective thrusts; however, particular focus is given to the two-thrust case, where an analytical solution, given certain assumptions, for the thrust components and firing times is available.

The maintenance of spacecraft formations via the control of differential orbital elements was first investigated by Schaub et al.,[3] who proposed a Lyapunov-based continuous-time control law. While effective, the continuous thrusting strategy is undesirable for most scientific missions because of the vibrations that the spacecraft would experience due to the thrusting. Impulsive control schemes remedy the vibrations

Spacecraft Dynamics and Control Laboratory, University of Toronto Institute for Aerospace Studies, Toronto, Canada

Corresponding author:
Christopher Damaren, Spacecraft Dynamics and Control Laboratory, University of Toronto Institute for Aerospace Studies, 4925 Dufferin Street, Toronto M3H 5T6, Canada.
Email: damaren@utias.utoronto.ca

problem. Impulsive formation controllers using near-circular orbit approximations have been developed for long-term formation keeping[4] and implemented for formation flying missions currently in orbit.[5–7] For formations with non-zero eccentricities, a three-impulse formation keeping strategy has been developed by Schaub et al.[8]

Model predictive controllers based on both relative Cartesian states and differential elements have been developed for control of formations in eccentric orbits in Tillerson and How[9] and Breger and How.[10] These methods can be formulated to be robust to sensor noise and other disturbances; however, they are ultimately numerical optimization problems and their requisite computational load may not be feasible or desirable for some missions.

The control scheme presented in this article extends the strategy for circular orbits proposed by Vadali et al.[4] to non-circular orbits. It will be shown that by including the effects of the J_2 perturbation into the controller design, superior relative position control and ΔV cost compared to Schaub et al.'s general three-impulse strategy can be achieved. A full derivation of the control strategy constraint equations is presented, followed by performance results from implementation of the controller in simulation of the nonlinear spacecraft dynamics. For the two-impulse case in particular, the stability of the closed-loop system is assessed using a discrete-time system describing the evolution of the differential element error. Stability predictions from the discrete-time model are corroborated with results from simulation of the nonlinear equations.

Problem formulation

The objective of any formation flying control strategy is to maintain the desired relative position of the deputy spacecraft with respect to a chief spacecraft. An intuitive frame of reference to express the relative position of the deputy spacecraft, $\mathbf{r} = [r_r \; r_\theta \; r_h]^{\mathbf{T}}$, is the local-vertical local-horizontal (LVLH) reference frame, illustrated in Figure 1, where $\hat{\mathbf{h}}_r$ is in the direction of the position vector of the chief spacecraft, outward from the Earth, $\hat{\mathbf{h}}_h$ is normal to the orbital plane, and $\hat{\mathbf{h}}_\theta$ completes the right-hand rule.

The relative orbit of the deputy spacecraft can also be described by the difference between its mean orbital elements and the mean orbital elements of the chief spacecraft

$$\delta \boldsymbol{e} = \boldsymbol{e}_d - \boldsymbol{e}_c \tag{1}$$

where the classical mean orbital elements are

$$\boldsymbol{e} = [\, a \quad e \quad i \quad \Omega \quad \omega \quad M \,] \tag{2}$$

Rather than having a time-varying position trajectory, by using differential mean elements, a formation geometry can be represented by six time-invariant (in the Keplerian case) differential elements. Mean elements, in particular, are a natural choice for formation control, since the secular effects of the J_2 zonal harmonic perturbation are included in their dynamics. Since relative position error is a more intuitive way of qualifying controller performance than differential element error, the relative position and velocity of the deputy spacecraft can be obtained via

$$\begin{bmatrix} \mathbf{r} \\ \dot{\mathbf{r}} \end{bmatrix} = \boldsymbol{\Sigma}(t)\mathbf{D}(t)\delta\mathbf{e}_{ns} \tag{3}$$

where $\mathbf{D}(t)$ is the first-order transformation between mean and osculating differential orbital elements and $\boldsymbol{\Sigma}(t)$ is the transformation between the osculating differential elements and the LVLH curvilinear

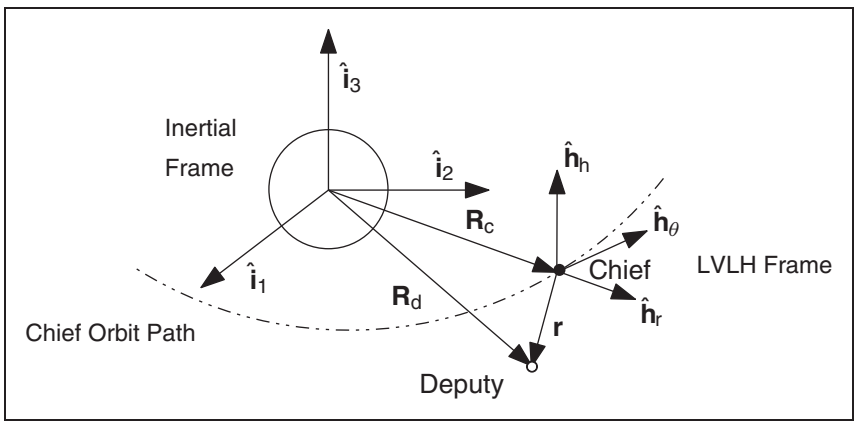

Figure 1. LVLH reference frame.
LVLH: local-vertical local-horizontal.

coordinate system. Both transformations can be found for the nonsingular differential element set

$$\delta \boldsymbol{e}_{ns} = \begin{bmatrix} \delta a & \delta i & \delta\Omega & \delta q_1 & \delta q_2 & \delta\theta \end{bmatrix}$$

in Gim and Alfriend.[11] To use the classical elements, a transformation between singular and nonsingular differential elements is needed

$$\delta \boldsymbol{e}_{ns} = \mathbf{N}(t)\delta \boldsymbol{e} \tag{4}$$

where

$$\mathbf{N}(t) = \begin{bmatrix} 1 & 0 & 0 & 0 & 0 & 0 \\ 0 & 0 & 1 & 0 & 0 & 0 \\ 0 & 0 & 0 & 1 & 0 & 0 \\ 0 & \cos\omega & 0 & 0 & -e\sin\omega & 0 \\ 0 & \sin\omega & 0 & 0 & e\cos\omega & 0 \\ 0 & \dfrac{\sin f(2+e\cos f)}{\eta^2} & 0 & 0 & 1 & \dfrac{(1+e\cos f)^2}{\eta^3} \end{bmatrix} \tag{5}$$

and $\eta = \sqrt{1-e^2}$.

J2 drift for formations in eccentric orbits

Although in high altitude orbits the strength of the the J_2 perturbation is diminished, drift in spacecraft formations due to the perturbation can still degrade formation geometry. This article considers two formations for the purpose of illustrating the proposed control methodology.

Highly eccentric orbit case – MMS formation. Spacecraft formation flying in high altitude, highly eccentric orbits (HEO) has been proposed for a number of upcoming missions. One of these missions, the MMS, will operate in an orbit with a semi-major axis of $a = 42{,}905$ km and eccentricities varying between $e = 0.81818$ and $e = 0.9084$.[12] Closed aperture formations operating in Molniya orbits with $a = 46{,}000$ km and $e = 0.67$ have been proposed for distributed Earth imaging applications.[13] Although, at these high orbits, the specific magnitude of the J_2 gravity perturbation is on the order of 1×10^{-6} N/kg, differences in the mean orbital element drift rates of the chief and deputy spacecraft can cause formation drift on the order of 1–100 m/orbit, depending on the formation.

Four spacecraft will eventually comprise the entire MMS formation. For simplicity, only two spacecraft are considered in this article. The two-spacecraft formation is defined by the initial conditions in Table 1. The formation is a closed, periodic formation with an average chief-deputy separation of 32 km. The growth in error in the relative position of the deputy spacecraft is illustrated in Figure 2. Drift is largest in radial and along-track directions, approaching position errors of 2 km and 5 km, respectively, over five orbits. Drift in the out-of-plane direction is an order of magnitude less, nearing 500 m of error after five orbits. The figure was generated by calculating the relative position of the deputy spacecraft after obtaining the inertial positions of both chief and deputy spacecraft by integration of the nonlinear equations of motion. The drift magnitudes correspond to the magnitudes predicted by differencing the mean element drift rates of chief and deputy spacecraft and transforming it to relative position error.

Table 1. MMS formation initial orbital elements.[12]

Chief			Deputy		
a,	km	42,905	δa,	m	−40.175
e		0.81818	δe,	10^{-3}	−1.944
i,	deg	28.5	δi,	deg, 10^{-4}	−1.593
Ω,	deg	357.8	$\delta\Omega$,	deg, 10^{-3}	−2.01
ω,	deg	298.2	$\delta\omega$,	deg, 10^{-3}	−9.50
M,	deg	0.0	δM,	deg, 10^{-2}	2.838

Mid-eccentric orbit case - elliptical PCO. This formation is a 1000 m elliptical projected circular orbit (PCO) formation flying at an eccentricity of 0.35. The initial conditions for the formation are provided in Table 2. The term elliptical is used to indicate that the relative motion is not perfectly circular, due to the moderate eccentricity of the chief spacecraft orbit. For this formation, maximum position error grows approximately 0.23 m per orbit.

Controller formulation

The dynamics of the mean orbital elements are

$$\dot{\boldsymbol{e}}(t) = \begin{bmatrix} 0 \\ 0 \\ 0 \\ \dot{\Omega} \\ \dot{\omega} \\ \dot{M} \end{bmatrix} + \begin{bmatrix} \dfrac{2a^2 e\sin f}{h} & \dfrac{2a^2 p}{rh} & 0 \\ \dfrac{p\sin f}{h} & \dfrac{(p+r)\cos f + re}{h} & 0 \\ 0 & 0 & \dfrac{r\cos\theta}{h} \\ 0 & 0 & \dfrac{r\sin\theta}{h\sin i} \\ -\dfrac{p\cos f}{he} & \dfrac{(p+r)\sin f}{he} & -\dfrac{r\sin\theta}{h\tan i} \\ \dfrac{b(p\cos f - 2re)}{ahe} & -\dfrac{b(p+r)\sin f}{ahe} & 0 \end{bmatrix} \times \begin{bmatrix} u_r(t) \\ u_\theta(t) \\ u_h(t) \end{bmatrix} \tag{6}$$

where $r = p/(1 + e\cos f)$ is the orbit radius and $h = abn$ is the orbital angular momentum. Gauss's variational equations (GVE) relate accelerations, $\mathbf{u}(t) = [u_r(t)\ u_\theta(t)\ u_h(t)]^{\mathrm{T}}$, expressed in the LVLH frame to changes in the the orbital elements. Although derived for osculating elements, the GVE are accurate to $\mathcal{O}(J_2)$ for mean elements.[14] The well-known secular drift rates of the mean elements are

$$\dot{a} = 0 \tag{7}$$

$$\dot{e} = 0 \tag{8}$$

$$\dot{i} = 0 \tag{9}$$

$$\dot{\Omega} = -\frac{3}{2}J_2 n\left(\frac{R_\oplus}{p}\right)^2 \cos i \tag{10}$$

$$\dot{\omega} = \frac{3}{4}J_2 n\left(\frac{R_\oplus}{p}\right)^2 (5\cos^2 i - 1) \tag{11}$$

$$\dot{M} = n + \frac{3}{4}J_2 n\eta\left(\frac{R_\oplus}{p}\right)^2 (3\cos^2 i - 1) \tag{12}$$

where $R_\oplus$ is the equatorial radius of the Earth and J_2 is the second zonal harmonic coefficient.

The orbital element dynamics can be written in the form

$$\dot{\boldsymbol{e}} = \mathbf{A}(\boldsymbol{e}) + \mathbf{B}(\boldsymbol{e})\mathbf{u}(t) \tag{13}$$

where $\mathbf{A}(\boldsymbol{e}) = [0\ 0\ 0\ \dot{\Omega}\ \dot{\omega}\ \dot{M}]^{\mathrm{T}}$, $\mathbf{u}(t) = [u_r\ u_\theta\ u_h]^{\mathrm{T}}$, and $\mathbf{B}(\boldsymbol{e})$ is the coefficient matrix of $\mathbf{u}(t)$ in equation (6) and the mean elements $\boldsymbol{e}$ are implicitly a function of time, t. The dynamics of the deputy mean differential elements are therefore

$$\begin{aligned}\delta\dot{\boldsymbol{e}} = \dot{\boldsymbol{e}}_d - \dot{\boldsymbol{e}}_c, &= \mathbf{A}(\boldsymbol{e}_c + \delta\boldsymbol{e}) - \mathbf{A}(\boldsymbol{e}_c) \\ &+ \mathbf{B}(\boldsymbol{e}_c + \delta\boldsymbol{e})\mathbf{u}_d - \mathbf{B}(\boldsymbol{e}_c)\mathbf{u}_c\end{aligned} \tag{14}$$

The chief spacecraft is assumed to be uncontrolled, so $\mathbf{u}_c = \mathbf{0}$. The deputy element dynamics are linearized about the chief mean orbital elements to yield

$$\delta\dot{\boldsymbol{e}} \simeq \left.\frac{\partial\mathbf{A}}{\partial\boldsymbol{e}}\right|_{e=e_c}\delta\boldsymbol{e} + \left(\mathbf{B}(\boldsymbol{e}_c) + \left.\frac{\partial\mathbf{B}}{\partial\boldsymbol{e}}\right|_{e=e_c}\delta\boldsymbol{e}\right)\mathbf{u}_d \tag{15}$$

Since there is no bound on $\delta\boldsymbol{e}$, the term $\left.\frac{\partial\mathbf{B}}{\partial\boldsymbol{e}}\right|_{e_c}\delta\boldsymbol{e}$ can be arbitrarily large. As Breger and How show in Breger and How,[10] for sufficiently small $\delta\boldsymbol{e}$, the term is small compared to to $\mathbf{B}(\boldsymbol{e}_c)$ and can be safely neglected. While the definition of 'sufficiently small' is dependent on the formation, typically for spacecraft near their desired differential element, the assumption that $\delta\boldsymbol{e}$ is sufficiently small is a reasonable one. The matrix $\tilde{\mathbf{A}}(\boldsymbol{e}) \equiv \left.\frac{\partial\mathbf{A}}{\partial\boldsymbol{e}}\right|_{\boldsymbol{e}}$ is a 6×6 matrix of the form

$$\tilde{\mathbf{A}} = \left[\begin{array}{ccc|c} \multicolumn{3}{c|}{\mathbf{0}_{3\times3}} & \mathbf{0}_{3\times3} \\ \hline \frac{\partial\dot{\Omega}}{\partial a} & \frac{\partial\dot{\Omega}}{\partial e} & \frac{\partial\dot{\Omega}}{\partial i} & \\ \frac{\partial\dot{\omega}}{\partial a} & \frac{\partial\dot{\omega}}{\partial e} & \frac{\partial\dot{\omega}}{\partial i} & \mathbf{0}_{3\times3} \\ \frac{\partial\dot{M}}{\partial a} & \frac{\partial\dot{M}}{\partial e} & \frac{\partial\dot{M}}{\partial i} & \end{array}\right] \tag{16}$$

Table 2. Elliptical PCO formation closed-aperture formation initial orbital elements.

Chief			Deputy		
a,	km	17,200	δa,	m	−0.343
e		0.35	δe		0.0
i,	deg	20.0	δi,	deg, 10^{-3}	3.502
Ω,	deg	0.0	$\delta\Omega$,	deg, 10^{-3}	1.805
ω,	deg	10.0	$\delta\omega$,	deg, 10^{-3}	−6.455
M,	deg	0.0	δM,	deg, 10^{-3}	4.458

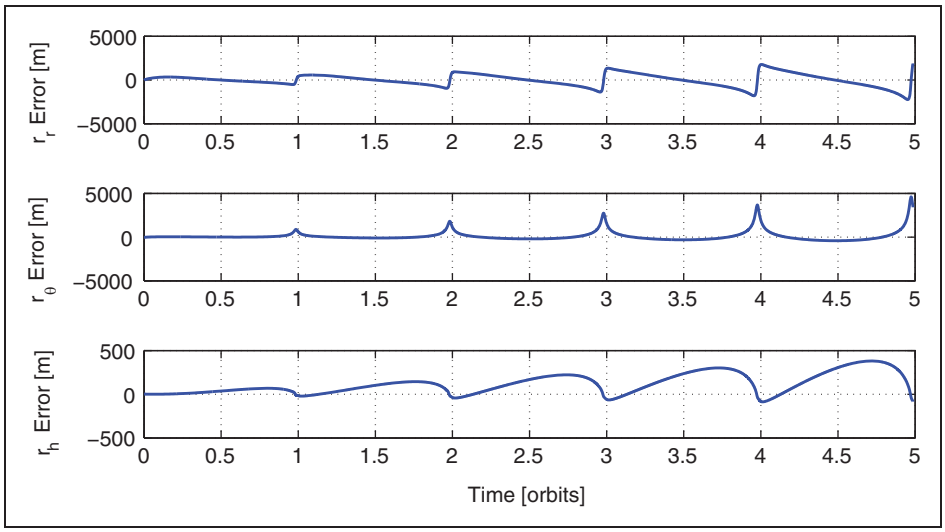

Figure 2. Relative position drift of a formation in HEO.

where the only non-zero elements are the partial derivatives of the mean element drift rates with respect to a, e, and i. Assuming that over a time interval t_0 to t_f there are N impulsive control thrusts $\Delta\mathbf{v}_1,\ldots,\Delta\mathbf{v}_N$ that are applied at t_i, $i=1,\ldots,N$, then the dynamics of the system are

$$\delta\dot{\boldsymbol{e}}(t)=\tilde{\mathbf{A}}(\boldsymbol{e}_c)\delta\boldsymbol{e}(t)+\sum_{i=1}^{N}\mathbf{B}(\boldsymbol{e}_c)\mathbf{u}_i(t)\delta(t-t_i) \tag{17}$$

where $\delta(\cdot)$ is the dirac delta function. It is assumed that the durations of the corrective thrusts are sufficiently small, as to be considered instantaneous. Integrating equation (17) from t_0 to t_f yields an analytical expression for the evolution of the differential orbital elements

$$\delta\boldsymbol{e}(t_f)=e^{\tilde{\mathbf{A}}(\boldsymbol{e}_c)\Delta t_{f0}}\delta\boldsymbol{e}(t_0)+\sum_{i=1}^{N}e^{\tilde{\mathbf{A}}(\boldsymbol{e}_c)\Delta t_{fi}}\mathbf{B}(\boldsymbol{e}_c(t_i))\Delta\mathbf{v}_i, \tag{18}$$

where $\Delta t_{ji}=t_j-t_i$ and $e^{\tilde{\mathbf{A}}(\boldsymbol{e}_c)}$ is the matrix exponential of $\tilde{\mathbf{A}}$ evaluated at $\boldsymbol{e}_c$. The matrix $\tilde{\mathbf{A}}$ is nilpotent, such that $\tilde{\mathbf{A}}^k=0$ for $k\geqslant 2$. Using this property, the matrix exponential can be accurately evaluated by

$$e^{\tilde{\mathbf{A}}(\boldsymbol{e}_c)\Delta t_{ji}}=\mathbf{1}+\tilde{\mathbf{A}}(\boldsymbol{e}_c)\Delta t_{ji} \tag{19}$$

Replacing the matrix exponential term in the vector $\delta\boldsymbol{e}(t_f)-e^{\tilde{\mathbf{A}}\Delta t_{f0}}\delta\boldsymbol{e}(t_0)$ by equation (19) yields

$$\delta\boldsymbol{e}(t_f)-e^{\tilde{\mathbf{A}}\Delta t_{f0}}\delta\boldsymbol{e}(t_0)=\delta\boldsymbol{e}(t_f)-\delta\boldsymbol{e}(t_0)-\tilde{\mathbf{A}}(\boldsymbol{e}_c)\delta\boldsymbol{e}(t_0)\Delta t_{f0} \tag{20}$$

Equation (20) suggests a feedback control law where $\delta\boldsymbol{e}(t_f)$ are the desired end states of the differential orbital elements and $\delta\boldsymbol{e}(t_0)$ are the current differential elements. The expanded individual equations from equation (18) for $N=2$ are presented in equations (21a) to (21f)

$$\delta a(t_f) = \delta a(t_0)+2\frac{a^2}{h}\sum_{j=1}^{2}\begin{bmatrix} e\sin f_j & \frac{p}{r_j} & 0\end{bmatrix}\Delta\mathbf{v}_j \tag{21a}$$

$$\delta e(t_f) = \delta e(t_0)+\sum_{j=1}^{2}\begin{bmatrix}\frac{p\sin f_j}{h} & \frac{(p+r)\cos f_j+r_j e}{h} & 0\end{bmatrix}\Delta\mathbf{v}_j \tag{21b}$$

$$\delta i(t_f) = \delta i(t_0)+\sum_{j=1}^{2}\begin{bmatrix}0 & 0 & \frac{r_j\cos\theta_j}{h}\end{bmatrix}\Delta\mathbf{v}_j \tag{21c}$$

$$\begin{aligned}\delta\Omega(t_f)=\delta\Omega(t_0)&+\left(\frac{\partial\dot{\Omega}}{\partial a}\delta a(t_0)+\frac{\partial\dot{\Omega}}{\partial e}\delta e(t_0)+\frac{\partial\dot{\Omega}}{\partial i}\delta i(t_0)\right)\Delta t_{f0}\\&+\sum_{j=1}^{2}\begin{bmatrix}0 & 0 & \frac{r_j\sin\theta_j}{h\sin i}\end{bmatrix}\Delta\mathbf{v}_j\\&+\left(\frac{\partial\dot{\Omega}}{\partial a}\Delta\delta a_{fj}+\frac{\partial\dot{\Omega}}{\partial e}\Delta\delta e_{fj}+\frac{\partial\dot{\Omega}}{\partial i}\Delta\delta i_{fj}\right)\Delta t_{fj}\end{aligned} \tag{21d}$$

$$\begin{aligned}\delta\omega(t_f)=\delta\omega(t_0)&+\left(\frac{\partial\dot{\omega}}{\partial a}\delta a(t_0)+\frac{\partial\dot{\omega}}{\partial e}\delta e(t_0)+\frac{\partial\dot{\omega}}{\partial i}\delta i(t_0)\right)\Delta t_{f0}\\&+\sum_{j=1}^{2}\begin{bmatrix}-\frac{p\cos f_j}{he} & \frac{(p+r_j)\sin f_j}{he} & -\frac{r_j\sin\theta}{h\tan i}\end{bmatrix}\Delta\mathbf{v}_j\\&+\left(\frac{\partial\dot{\omega}}{\partial a}\Delta\delta a_{fj}+\frac{\partial\dot{\omega}}{\partial e}\Delta\delta e_{fj}+\frac{\partial\dot{\omega}}{\partial i}\Delta\delta i_{fj}\right)\Delta t_{fj}\end{aligned} \tag{21e}$$

$$\begin{aligned}\delta M(t_f)=\delta M(t_0)&+\left(\frac{\partial\dot{M}}{\partial a}\delta a(t_0)+\frac{\partial\dot{M}}{\partial e}\delta e(t_0)+\frac{\partial\dot{M}}{\partial i}\delta i(t_0)\right)\Delta t_{f0}\\&+\sum_{j=1}^{2}\begin{bmatrix}\frac{b(p\cos f_j-2r_j e)}{ahe} & \frac{b(p+r_j)\sin f_j}{ahe} & 0\end{bmatrix}\Delta\mathbf{v}_j\\&+\left(\frac{\partial\dot{M}}{\partial a}\Delta\delta a_{fj}+\frac{\partial\dot{M}}{\partial e}\Delta\delta e_{fj}+\frac{\partial\dot{M}}{\partial i}\Delta\delta i_{fj}\right)\Delta t_{fj}\end{aligned} \tag{21f}$$

For $N>2$ impulses, the thrust components and firing times can be determined by solving the optimization problem

$$\begin{aligned}\text{minimize}\quad & \sum_{j=1}^{N}\Delta\mathbf{v}_j{}^{\mathrm{T}}\Delta\mathbf{v}_j\\ \text{with respect to}\quad & \Delta\mathbf{v}_j, t_j,\quad j=1,\ldots,N\\ \text{subject to}\quad & \mathbf{0}=\delta\boldsymbol{e}(t_f)-e^{\tilde{\mathbf{A}}(\boldsymbol{e}_c)\Delta t_{f0}}\delta\boldsymbol{e}(t_0)\\&\qquad -\sum_{j=1}^{N}e^{\tilde{\mathbf{A}}(\boldsymbol{e}_c)\Delta t_{fj}}\mathbf{B}(\boldsymbol{e}_c(t_j))\Delta\mathbf{v}_j.\end{aligned}$$

For the case of $N=2$ impulses, equation (21a) to (21f) can yield additional insight into the control problem that offers an alternative analytical method for calculating a thrust solution. This will be explored in the following section.

The two-impulse case

For two control thrusts at arbitrary times t_1 and t_2, where $t_0<t_1<t_2<t_f$, the impulse vectors $\Delta\mathbf{v}_1$ and $\Delta\mathbf{v}_2$ can be solved for

$$\begin{bmatrix}\Delta\mathbf{v}_1\\ \Delta\mathbf{v}_2\end{bmatrix}=\left[e^{\tilde{\mathbf{A}}(\boldsymbol{e}_c)\Delta t_{f1}}\mathbf{B}(\boldsymbol{e}_c(t_1))|e^{\tilde{\mathbf{A}}(\boldsymbol{e}_c)\Delta t_{f2}}\mathbf{B}(\boldsymbol{e}_c(t_2))\right]^{-1}\times\left(\delta\boldsymbol{e}(t_f)-e^{\tilde{\mathbf{A}}(\boldsymbol{e}_c)\Delta t_{f0}}\delta\boldsymbol{e}(t_0)\right) \tag{22}$$

For convenience, the matrix $\mathbf{X}(\boldsymbol{e}_c,\,t_1,\,t_2)$ is defined as

$$\mathbf{X}(\boldsymbol{e}_c,t_1,t_2)\equiv\left[e^{\tilde{\mathbf{A}}(\boldsymbol{e}_c)\Delta t_{f1}}\mathbf{B}(\boldsymbol{e}_c(t_1))|e^{\tilde{\mathbf{A}}(\boldsymbol{e}_c)\Delta t_{f2}}\mathbf{B}(\boldsymbol{e}_c(t_2))\right] \tag{23}$$

Alternatively, rather than choosing arbitrary thrust application times, a possible set of thrust application times can be calculated using equations (21c) and (21d). If the effects of changes to δa, δe, δi on the differential drift rate of the right ascension of the ascending node are momentarily ignored, equation (21d) becomes a function of the out-of-plane components of the thrust vectors Δv_{h_i}. Equation (21c) is already only a function of Δv_{h_i}. Using the two equations together, the true latitudes corresponding to the thrust application times and the out-of-plane thrust components can be calculated. The true latitude of the first thrust is calculated using

$$\tan\theta_1 = \frac{\left(\begin{array}{l}\left(\delta\Omega(t_f)-\delta\Omega(t_0)-\left(\frac{\partial\dot{\Omega}}{\partial a}\delta a(t_0)+\frac{\partial\dot{\Omega}}{\partial e}\delta e(t_0)\right.\right.\\ \left.\left.+\frac{\partial\dot{\Omega}}{\partial i}\delta i(t_0)\right)\Delta t_{f0}\right)\sin i\end{array}\right)}{\delta i(t_f)-\delta i(t_0)} \tag{24}$$

θ_1 must be adjusted to lie between 0 and π, then $\theta_2=\theta_1+\pi$. Using θ_1, the first out-of-plane thrust component is

$$\Delta v_{h_1} = \pm\frac{h}{2r_1}\left((\delta i(t_f)-\delta i(t_0))^2 + \left(\delta\Omega(t_f)-\delta\Omega(t_0)-\left(\frac{\partial\dot{\Omega}}{\partial a}\delta a(t_0) + \frac{\partial\dot{\Omega}}{\partial e}\delta e(t_0)+\frac{\partial\dot{\Omega}}{\partial i}\delta i(t_0)\right)\Delta t_{f0}\right)^2\sin^2 i\right)^{\frac{1}{2}} \tag{25}$$

If the original θ_1 is negative, the negative square root is taken for Δv_{h_1}, otherwise the positive root is taken. The second out-of-plane thrust component is $\Delta v_{h_2}=-\Delta v_{h_1}$. The remaining in-plane thrusts can be calculated by solving the remaining four constraint equations numerically.

Numerical simulation

To evaluate the proposed control scheme, the two formations described by Tables 1 and 2 are considered. The chief and deputy spacecraft are simulated using the full nonlinear equations of motion, with J_2 through J_6 gravitational perturbations included as disturbances. Rather than compensating for an initial error, the formation is initialized at the correct initial conditions and the controller corrects any drift in elements due to the gravitational perturbations.

The analytical two-impulse scheme, using equations (24) and (25), and an optimal four-impulse scheme are compared to Schaub et al's three-impulse scheme.[8] Four impulses are chosen to demonstrate the feasibility of using $N>2$ impulses for control. To obtain the four-impulse solution the MATLAB nonlinear optimization function `fmincon` is used to solve the optimization problem posed in the section 'Controller formulation'.

For both test cases described below ('MMS formation' and 'elliptical PCO formation') one orbital period was chosen for the control interval, so $t_0=0$ and $t_f=T$ where T is the orbit period $T=2\pi\sqrt{a^3/\mu}$.

MMS formation. Figure 3 illustrates the differential orbital element errors for the three control strategies. While Schaub et al.'s three-impulse strategy has minimal effect on differential semi-major axis and eccentricity, the strategies from this article cause periodic jumps in both differential elements, which may be undesirable. Due to the inclusion of the effect of J_2, however, the two and four-impulses schemes have improved tracking of the differential ascending node, argument of perigee, and significantly better tracking of mean anomaly.

This improved differential element tracking results in reduced relative position errors, as shown in Figure 4. For this case, the improvement is most pronounced in the along-track direction; however, all three directions have a superior tracking error. Relative position error statistics for the three cases are summarized in Table 3.

Total ΔV required for the two-impulse strategy is 12.0 mm/s and for Schaub's three-impulse strategy, it is 14.1 mm/s per orbit, while the optimal four-impulse strategy uses 6.97 mm/s per orbit. Overall, the four-impulse scheme has the best performance in this case, having both the lowest relative position tracking error and required ΔV. The two-impulse strategy has slightly larger error than the four-impulse strategy; however, its ΔV requirement is similar to that of Schaub's three-impulse scheme.

Elliptical PCO formation. Results similar to those seen for the MMS formation are seen for the elliptical PCO formation. Schaub's strategy tracks δa, δe and δi well for this case; however, its tracking of $\delta\Omega$, $\delta\omega$ and δM is worse than that of both proposed schemes. Differential element tracking errors for this case are presented in Figure 5. Position tracking error, presented in Figure 6, using Schaub's scheme is also inferior for all three position components. Required ΔV for control is compared in Figure 7. Schaub's strategy used no control for the first orbit, since the formation is initialized to the correct orbital elements. The proposed strategy does apply a control effort to compensate for the J_2 pertubration over that orbit. Over ten orbits, both the two-impulse and four-impulse scheme outperform Schaub's scheme in required control effort, requiring 0.31 mm/s and 0.27 mm/s, respectively, compared to 0.32 mm/s.

Effects of increasing N. The four-impulse case in the previous section was provided to demonstrate the

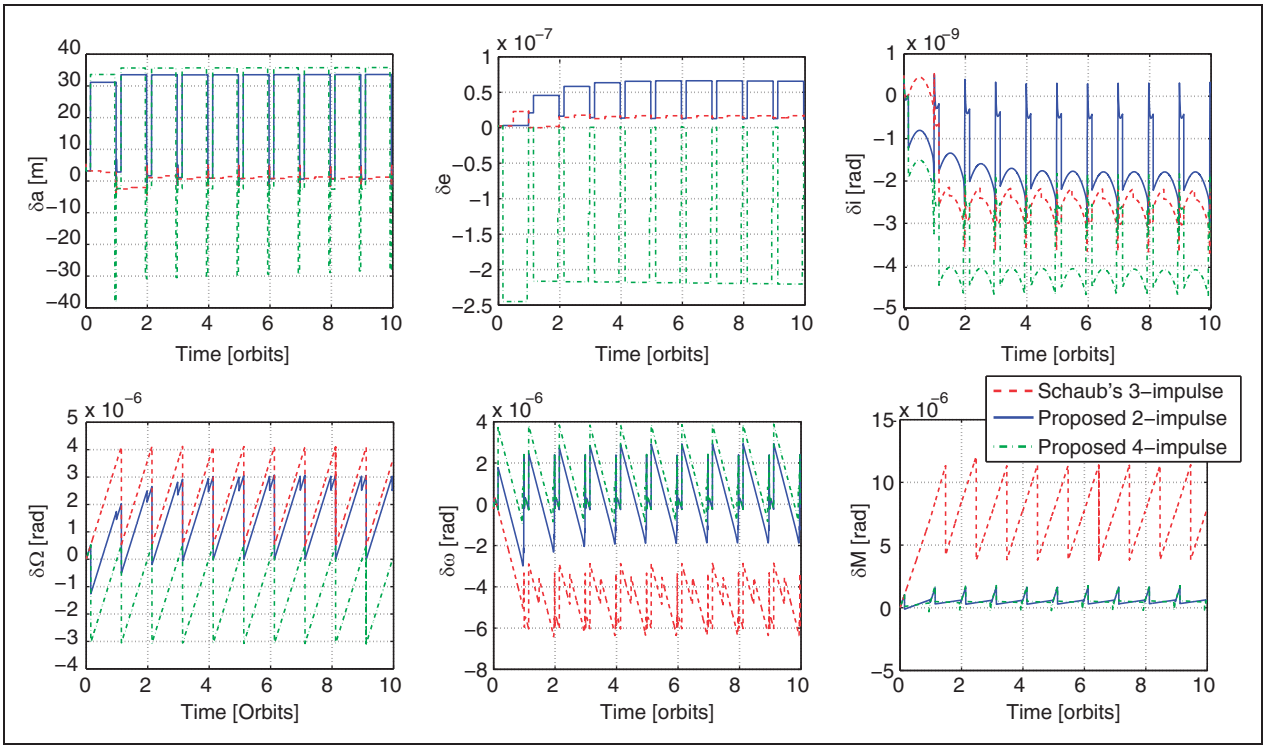

Figure 3. Comparison of differential element errors for the MMS formation.

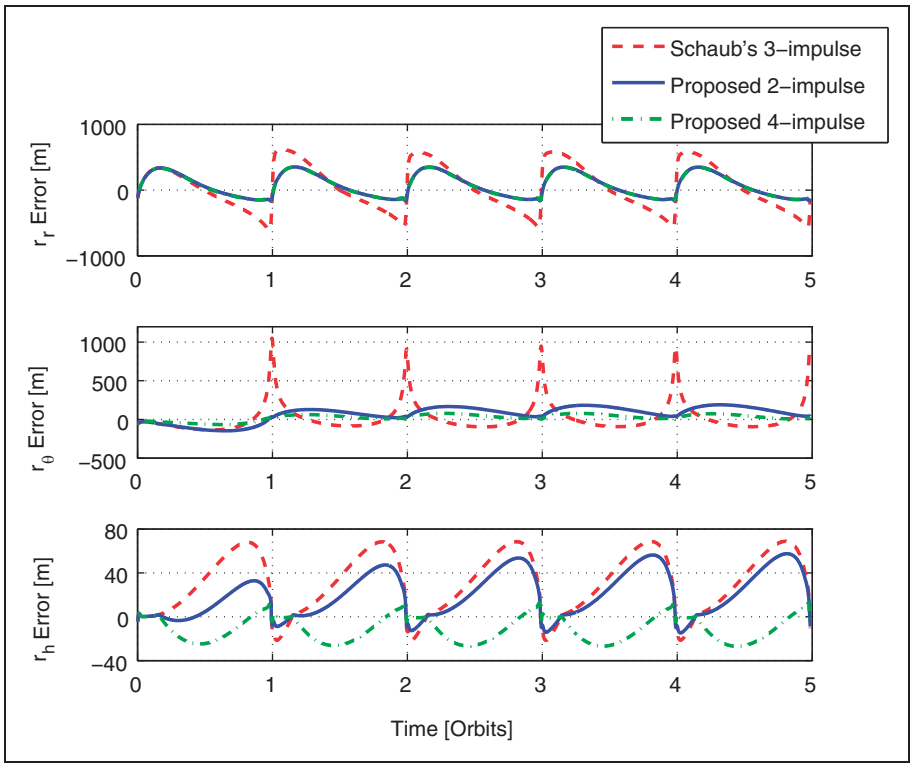

Figure 4. Comparison of relative position error for the MMS formation.

feasiblity of the controller for an abitrary number of thrusts. Although performance using a larger number of thrusts cannot be inferred from the previous case alone, it is not unreasonable to assume that as N grows the tracking error and required control effort will converge to a limiting, near-continuous thrusting case. Additional simulations with larger N confirm this assumption.

Table 3. Position error statistics for MMS formation.

	RMS error			Max absolute error		
Strategy	r_r (m)	r_θ (m)	r_h (m)	r_r (m)	r_θ (m)	r_h (m)
Proposed two-impulse	190	119	29	362	190	58
Proposed four-impulse	186	48	16	350	80	28
Schaub's three-impulse	346	195	41	614	1050	69

RMS: root mean square.

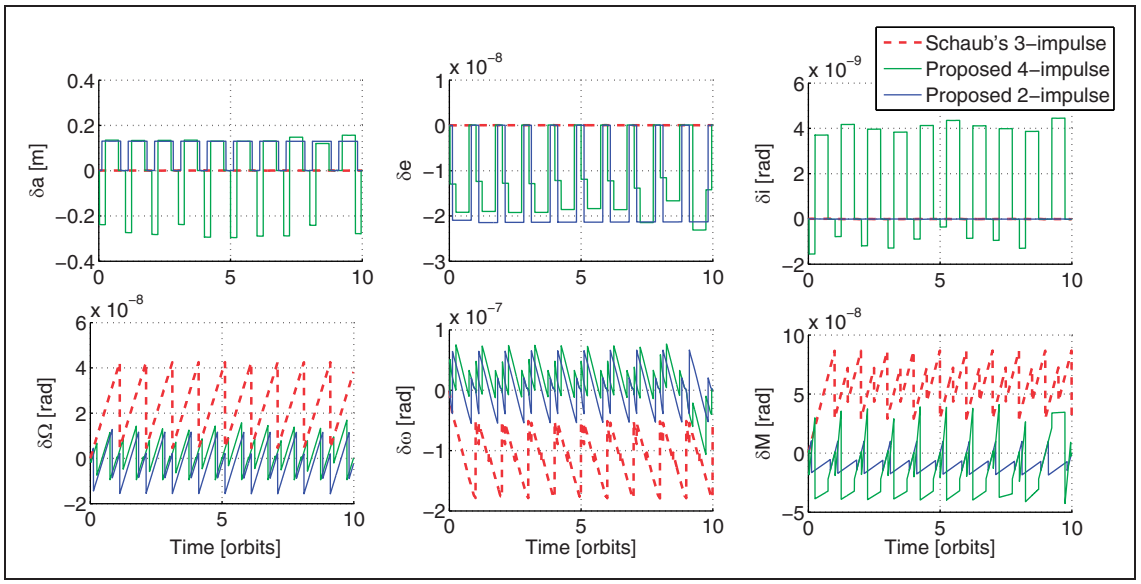

Figure 5. Differential element tracking error for the elliptical PCO formation.

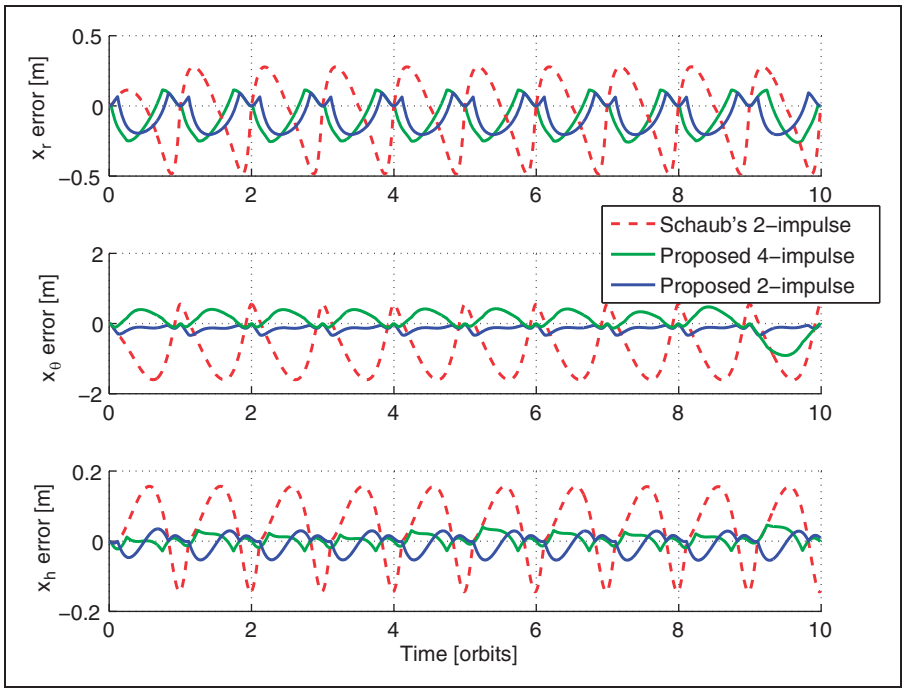

Figure 6. Comparison of relative position error for the elliptical PCO formation.

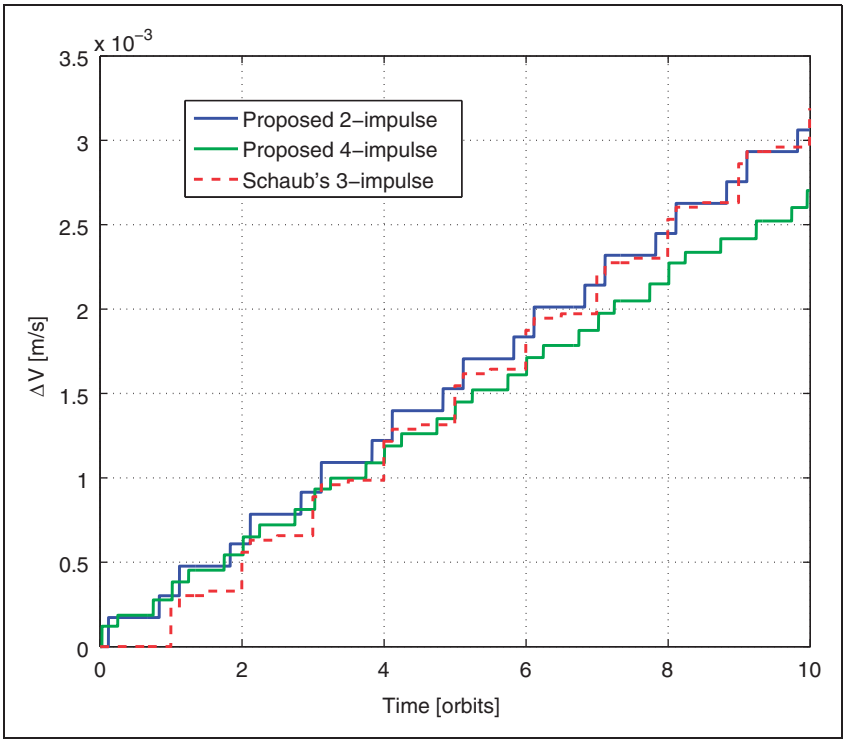

Figure 7. ΔV expenditure comparison for the elliptical PCO formation.

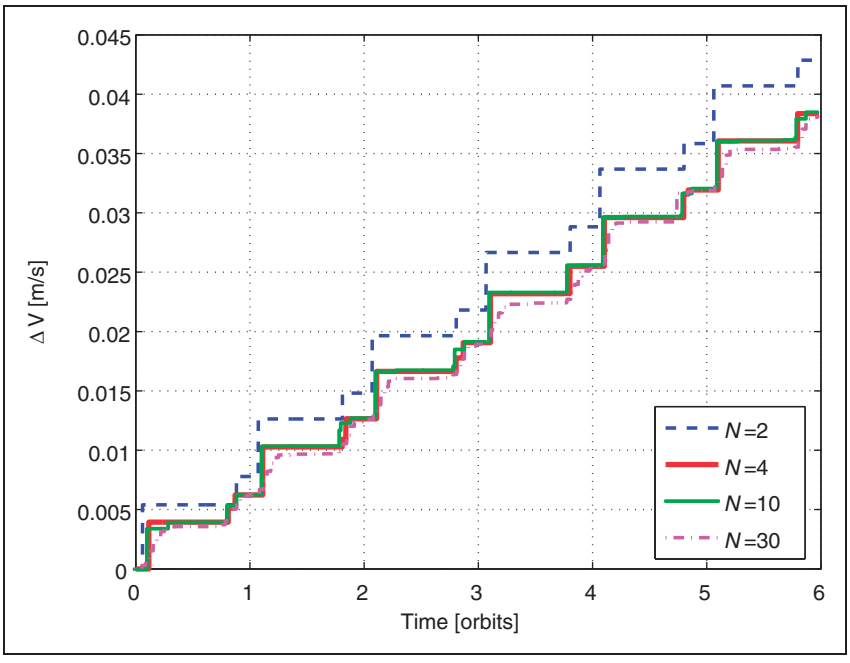

Figure 8. ΔV expenditure for different N.

Figure 8 compares the required control effort for the cases of $N = 2$, 4, 10, 30. An improvement in required ΔV is observed as N increases but beyond $N = 10$ the gain is minimal. Figure 9 shows how the tracking errors of δi and $\delta\omega$ change with different N. Some improvement is seen in the tracking of δi; however, the other element tracking errors behave similar to $\delta\omega$ tracking error, remaining approximately the same magnitude as the number of impulses increases.

How to determine an optimal N remains a subject for future work. It appears that there are benefits to an increased number of impulses per orbit, but the magnitude of the benefits will no doubt vary with the orbit of the chief spacecraft and the desired formation geometry. Determining an optimal N will not, however, be

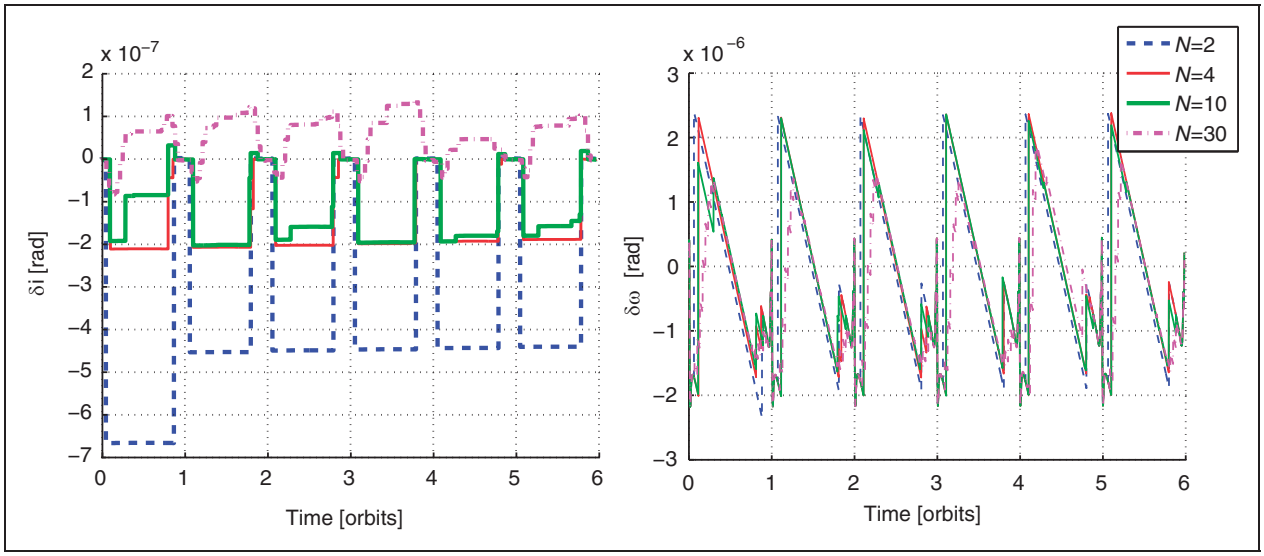

Figure 9. Error tracking for δi and $\delta\omega$ using different values for N.

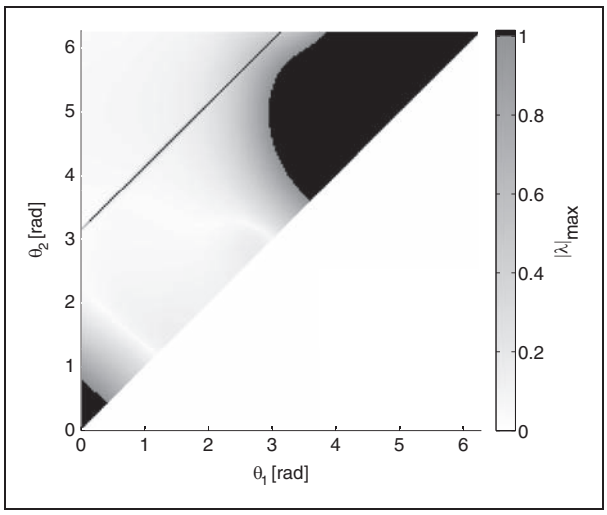

Figure 10. Stability plot: color denotes maximum eigenvalue magnitude.

only a question of improvement in control effort and error tracking. It will depend on the computational power available, since selecting a larger N will incur a penalty in terms of computation time.

The extent of the benefits offered by the N-impulse scheme may vary depending on the formation, but from the cases presented, the optimized strategy does provide both fuel savings and tracking improvement when compared to Schaub's three-impulse method.

Alternative optimal strategies. Breger and How[10] presents an optimal differential element-based model-predictive controller (MPC) for formation control. Compared to the MPC control, this article's optimized strategy is a smaller optimization problem, providing an optimal-per-orbit thrust solution while the MPC control provides a more robust, multi-orbit formation keeping plan, at the cost of increased computations.

The optimization problem in Breger and How[10] is, in general, a much larger optimization problem. A time arc is discretized into N nodes, with a corrective thrust being applied at each. Constraints on the differential element errors are enforced at each node. The method yields a formation keeping plan with N thrusts for N nodes in the time arc. By adding additional constraints, the controller in Breger and How[10] can be made robust to sensor noise. Firing times, however, are not decided optimally; rather, by discretizing the time arc into a sufficiently large number of nodes (e.g. Breger and How[10] discretizes a one orbit-long time arc into 1000 nodes – resulting in 3×1000 design variables), optimal thrusts can be determined for each of the discretized nodes. The assumption is that with a large N, some nodes will lie near optimal firing times. The need for this large number of discretization nodes significantly increases the complexity of the optimization problem.

In comparison, the presented optimization problem in this article determines both optimal thrusts and optimal firing times. A single error constraint is enforced at the end of the time arc. The inclusion of the firing time in the optimization problem means that there are $4N$ (three thrust components plus one firing time) design variables now, instead of $3N$, as in the case of Breger and How,[10] but N can be much smaller and optimal firing times will still be obtained. Choosing an 'optimal' N, as discussed previously, is still an open matter.

Formation stability for two-impulse control

The feedback law presented in equation (22) provides two corrective impulses for arbitrarily selected firing times. A natural question that arises is whether the chosen firing times result in a stable, closed-loop

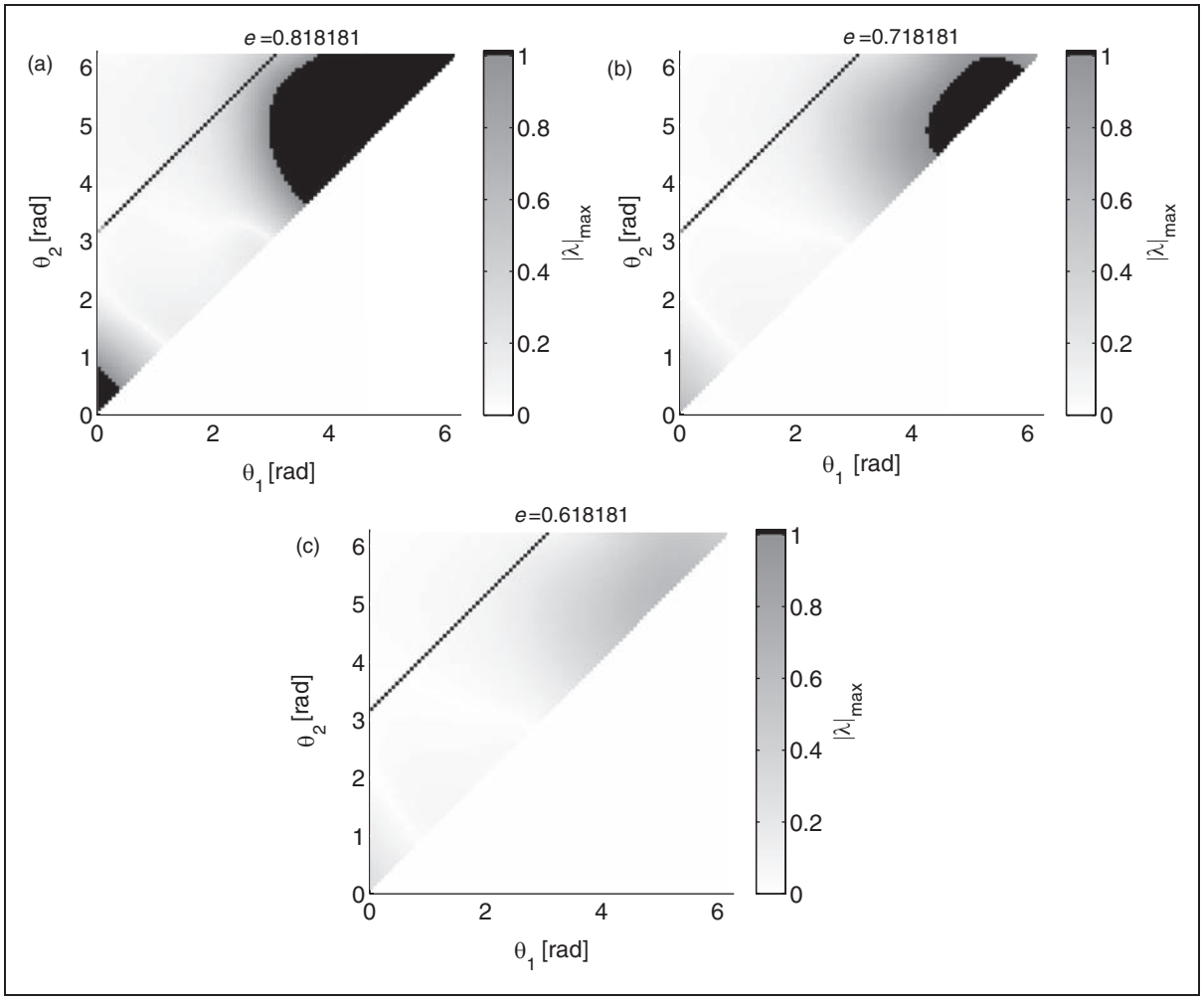

Figure 11. Changes to unstable regions due to eccentricity.

system. In this section, this question of input–output stability of the closed-loop formation using the feedback law from equation (22) is addressed.

Closed-loop discrete-time model

The mean orbital element tracking error is defined as

$$\boldsymbol{\zeta}(t) = \boldsymbol{e}_d(t) - \boldsymbol{e}_{d_R}(t) \tag{26}$$

which is equivalent to the differential orbital element tracking error

$$\begin{aligned}\boldsymbol{\zeta}(t) &= \delta\boldsymbol{e}_d(t) + \mathbf{e}_c(t) - \delta\boldsymbol{e}_{d_R}(t) - \boldsymbol{e}_c(t) \\ &= \delta\boldsymbol{e}(t) - \delta\boldsymbol{e}_R(t)\end{aligned} \tag{27}$$

Following the same linearization process as in the section 'Controller formulation', the error dynamics are

$$\dot{\boldsymbol{\zeta}}(t) = \tilde{\mathbf{A}}(\boldsymbol{e}_R)\boldsymbol{\zeta}(t) + \mathbf{B}(\boldsymbol{e}_R)\mathbf{u}(t), \tag{28}$$

where $\tilde{\mathbf{A}}$ and $\mathbf{B}(\boldsymbol{e})$ matrices are the same as in the section 'Controller formulation', but are here evaluated using the deputy's reference orbital elements. Assuming small thrust magnitudes that can be approximated as impulses, the system dynamics for the two-impulse case are

$$\begin{aligned}\dot{\boldsymbol{\zeta}}(t) = \tilde{\mathbf{A}}(\boldsymbol{e}_R)\boldsymbol{\zeta} &+ \mathbf{B}(\boldsymbol{e}_R(t_1))\mathbf{u}_1\delta(t-t_1) \\ &+ \mathbf{B}(\boldsymbol{e}_R(t_2))\mathbf{u}_2\delta(t-t_2)\end{aligned} \tag{29}$$

This assumption is a reasonable one, since the purpose of the control scheme is to maintain a current formation, not to perform any significant reconfigurations. Integrating equation (29), the evolution over time of the system is given by

$$\begin{aligned}\boldsymbol{\zeta}(t) &= e^{\tilde{\mathbf{A}}t}\boldsymbol{\zeta}(t_0) + \int_0^t e^{\tilde{\mathbf{A}}(t-\tau)}\mathbf{B}(t_1)\mathbf{u}_1\delta(\tau-t_1)\mathrm{d}\tau \\ &\quad + \int_0^t e^{\tilde{\mathbf{A}}(t-\tau)}\mathbf{B}(t_2)\mathbf{u}_2\delta(\tau-t_2)\mathrm{d}\tau \\ &= e^{\tilde{\mathbf{A}}t}\boldsymbol{\zeta}(t_0) + e^{\tilde{\mathbf{A}}(t-t_1)}\mathbf{B}(t_1)\Delta\mathbf{v}_1 \\ &\quad + e^{\tilde{\mathbf{A}}(t-t_2)}\mathbf{B}(t_2)\Delta\mathbf{v}_2\end{aligned} \tag{30}$$

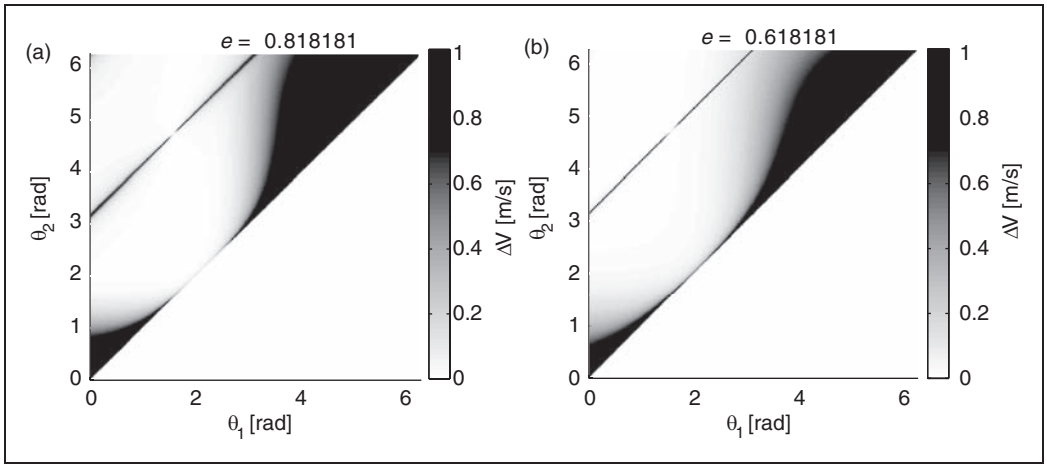

Figure 12. Estimated fuel usage, MMS formation.

where δ is the dirac delta function. An interval of one orbital period of the chief spacecraft, $T = 2\pi\sqrt{a^3/\mu}$, is considered. Discretizing equation (30) yields the following discrete-time system

$$\begin{aligned}\boldsymbol{\zeta}[k+1] &= e^{\tilde{\mathbf{A}}T}\boldsymbol{\zeta}[k] \\ &\quad + \left[\, e^{\tilde{\mathbf{A}}(T-t_1)}\mathbf{B}(t_1) | e^{\tilde{\mathbf{A}}(T-t_2)}\mathbf{B}(t_2) \,\right]\begin{bmatrix}\Delta\mathbf{v}_1 \\ \Delta\mathbf{v}_2\end{bmatrix} \\ &= \mathbf{A}_d\boldsymbol{\zeta}[k] + \mathbf{B}_d\Delta\mathbf{v}[k] \end{aligned} \tag{31}$$

Returning to the two-impulse control law in equation (22), $\delta\boldsymbol{e}(t_f) - \delta\boldsymbol{e}(t_0)$ is equivalent to $-\boldsymbol{\zeta}$, so the expression for the control vector $\Delta\mathbf{v}[k]$ can be obtained using

$$\Delta\mathbf{v}[k] = -\mathbf{X}^{-1}(\boldsymbol{e}_c, t_1, t_2)\Big(\boldsymbol{\zeta} + \tilde{\mathbf{A}}(\boldsymbol{e}_c)\delta\boldsymbol{e}(t_0)T\Big) \tag{32}$$

Substituting equation (32) into equation (31) gives an analytical description of the closed-loop system

$$\begin{aligned}\boldsymbol{\zeta}[k+1] = &\ (\mathbf{A}_d - \mathbf{B}_\mathrm{d}\mathbf{X}^{-1}(\boldsymbol{e}_c, t_1, t_2))\boldsymbol{\zeta}[k] \\ &- \mathbf{B}_d\mathbf{X}^{-1}(\boldsymbol{e}_c, t_1, t_2)\tilde{\mathbf{A}}(\boldsymbol{e}_c)\delta\boldsymbol{e}(t_0)T \end{aligned} \tag{33}$$

For bounded-input bounded-output stability

$$|\lambda_i| < 1, \qquad i = 1 \ldots 6,$$

where λ_i are the eigenvalues of the closed-loop state matrix $\mathbf{A}_d - \mathbf{B}_d\mathbf{X}^{-1}(\boldsymbol{e}_c,\ t_1,\ t_2)$.

Numerical example

The stability criteria presented above will hold true if the maximum eigenvalue in modulus, $\lambda_m = \max\{|\lambda_i|: \forall i \in [1,\ 6]\}$, is less than 1. An eigenvalue map of λ_m can be constructed for all possible firing time pairs, $\boldsymbol{\theta} = \{\theta_1,\ \theta_2\} \in [0,\ 2\pi)$ and $\theta_2 \neq \theta_1$, to illustrate possible regions of instability where the maximum eigenvalue modulus lies outside the unit disc. Firing time pairs $\boldsymbol{\theta}$ are specified in terms of chief true latitude.

The stability of the MMS formation from the section 'Numerical simulation' is considered. Figure 10 is the maximum eigenvalue in modulus plot for possible firing times. The plot is symmetric about the line $\theta_2 = \theta_1$, so only the upper half of the plot has been populated with data. There are three distinct regions where the selected firing times result in an unstable system. The region about the line $\theta_2 = \theta_1 + \pi$ is a result of the matrix $\mathbf{X}(\boldsymbol{e}_c,\ t_1,\ t_2)$ becoming ill-conditioned when θ_1 and θ_2 are separated by π. The condition number of $\mathbf{X}$ increases by several orders of magnitude and its inversion leads to out-of-plane thrust components that are excessively large. Numerical simulations of a formation using the unstable firing pairs validate the stability prediction. Note that in the analytical two-impulse case (the decoupled solution of the section 'The two-impulse case'), we used $\theta_2 = \theta_1 + \pi$ but this does not lead to instability on account of the approximations made there. The approximations make decoupling possible but avoid instability by providing a solution, which is slightly inconsistent with inverting the matrix $\mathbf{X}$.

The eccentricity of the chief orbit plays a role in the size of the unstable regions. As shown in Figure 11, lower chief eccentricities result in smaller unstable regions. Below a critical eccentricity, the unstable regions disappear entirely, except for the unstable region due to the ill-conditioned $\mathbf{X}$ matrix when firing times $\theta_2 = \theta_1 + \pi$.

An important consideration that has so far been ignored in the stability analysis is the ΔV needed for formation maintenance, given a firing time pair. The required ΔV changes significantly depending on what firing times are chosen and in some cases, due to its large magnitude, can invalidate the assumption of small impulsive thrusts. Figure 12(a) shows that while for the majority of firing time pairs the ΔV required is small, for some firing time pairs ΔV approaches 1 m/s.

For a 1 N hydrazine thruster, of a kind comparable to the ones uses aboard the PRISMA formation flying

mission,[15] a 1 m/s change in velocity would require about a two and a half minute thrust, assuming a 150 kg spacecraft. Such a burn can no longer be considered impulsive. Therefore the stability analysis for that firing time pair is no longer accurate. This case can be seen by comparing Figures 9(c) and 12(b), where a large region of firing times that are stable still have large ΔV requirements. Simulations show that firing time pairs with very large ΔV are unstable when the dynamics of a 1 N hydrazine thruster with an minimum impulse bit of 0.043 N are included in the simulation. The problem is essentially one of actuator saturation, where the desired control effort can no longer be applied at the required time. The stability analysis is therefore limited to firing time pairs whose thrusts are sufficiently small to be considered impulsive.

Conclusion

An impulsive control strategy has been presented to mitigate formation drift due to the J_2 perturbation for spacecraft formations in eccentric orbits. This work generalized the circular impulsive control scheme presented by Vadali et al. in previous work. The control strategy can be extended to mitigate the influence of higher order perturbations by including their effects on differential mean elements in the formulation of the constraint equations. Formation control has been demonstrated for both the analytically obtained two-impulse strategy and the numerically obtained four-impulse strategy. Performance compared to Schaub et al.'s existing three impulse control strategy showed improved mean different element tracking and, consequently, improved relative position tracking when using both analytical and numerical methods. Fuel costs for the two-impulse strategy were not significantly different from the three-impulse strategy; however, the optimized four-impulse control strategy did yield an improvement in required ΔV, in addition to having superior error tracking. The developed stability analysis shows that the majority of possible firing times are stable and viable for formation keeping, although some have prohibitively high fuel requirements. The stability analysis is valid under the assumption of thrusts that are sufficiently small to be considered impulsive.

Funding

The research was funded by a Discovery Grant from the Natural Sciences and Engineering Research Council of Canada.

References

1. Curtis S. The magnetospheric multiscale mission resolving fundamental processes in space plasmas. Technical Report, Report of the NASA Science and Technology Definition Team for the MMS Mission, 1999.
2. Lamy P and Vivs S. New perspective in solar coronal physics: giant externally occulted coronagraph using satellites in formation flight. *Acta Astronaut* 2009; 65: 273–278.
3. Schaub H, Vadali SR, Junkins JL, et al. Spacecraft formation flying control using mean orbit elements. *J Astronaut Sci* 2000; 48: 69–87.
4. Vadali SR, Yan H and Alfriend KT. Formation maintenance and fuel balancing for satellites with impulsive control. In: *Astrodynamics specialist conference and exhibit*, Honolulu, Hawaii, 2008.
5. D'Amico S, Gill E and Montenbruck O. Relative orbit control design for the PRISMA formation flying mission. In: *AIAA guidance, navigation and control conference and exhibit*, Keystone, Colorado, 2006.
6. Gill E, D'Amico S and Montenbruck O. Autonomous formation flying for the PRISMA mission. *J Spacecr Rockets* 2007; 44: 671–681.
7. Ardaens JS and D'Amico S. Spaceborne autonomous relative control system for dual satellite formations. *J Guid Contr Dynam* 2009; 32: 1859–1870.
8. Schaub H and Alfriend KT. Impulsive feedback control to establish specific mean orbit elements of spacecraft formations. *J Guid Contr Dynam* 2001; 24: 739–745.
9. Tillerson M and How JP. Formation flying control in eccentric orbits. In: *AIAA guidance, navigation, and control conference and exhibit*. Montreal, Canada, August 2001.
10. Breger L and How JP. Gauss's variational equation-based dynamics and control for formation flying spacecraft. *J Guid Contr Dynam* 2007; 30: 437–448.
11. Gim D-W and Alfriend K. State Transition matrix of relative motion for the perturbed noncircular reference orbit. *J Guid Contr Dynam* 2003; 26: 956–971.
12. Roscoe C, Vadali S, Alfriend K, et al. Optimal formation design for magnetospheric multiscale mission using differential orbital elements. *J Guid Contr Dynam* 2011; 34: 1070–1080.
13. Inalhan G, Tillerson M and How JP. Relative dynamics and control of spacecraft formations in eccentric orbits. *J Guid Contr Dynam* 2002; 25: 48–59.
14. Schaub H and Junkins JL. *Analytical mechanics of space systems*. Reston VA: American Institute of Aeronautics and Astronautics, 2003.
15. Persson S, Bodin P, Gill E, et al. PRISMA – an autonomous formation flying mission. In: *ESA small satellite systems and services symposium*, Sardinia, Italy, September 2006, pp.25–29.

Appendix

Notation

a	semi-major axis
b	semi-minor axis
e	eccentricity
$\mathbf{e}$	mean orbital element vector
f	true anomaly
i	inclination
M	mean anomaly
n	orbital angular velocity
r	orbit radius
$\mathbf{r}$	relative position vector

$\dot{\mathbf{r}}$	relative velocity vector
$\Delta\mathbf{v}$	impulsive thrust vector
Ω	right ascension of ascending node
ω	argument of periapsis
$\theta = \omega + f$	true latitude
$\delta(\cdot)$	differential quantity
$\hat{(\cdot)}$	unit quantity

Subscript

c	chief
d	deputy
h	out-of-plane direction
ns	nonsingular
r	radial direction
R	reference
θ	along-track direction
$\oplus$	earth-related

Superscript

$*$	optimal solution